JOURNAL OF COMPUTATIONAL PHYSICS 50, 101–115 (1983)

Numerical Optimization Studies of Axisymmetric Unsteady Sprays

S. K. AGGARWAL, G. J. FIX, D. N. LEE, AND W. A. SIRIGNANO

Carnegie–Mellon University, Pittsburgh, Pennsylvania 15213

Received May 27, 1981; revised September 14, 1982

A hybrid numerical technique is developed for the treatment of axisymmetric unsteady spray equations. An Eulerian mesh is employed for the parabolic gas-phase subsystem of equations while a Lagrangian scheme (or method of characteristics) is utilized for the droplet equations. The integration schemes and the scheme for interpolation between the two meshes are demonstrated to be second-order accurate. The approach is shown to be especially useful in situations where a multivaluedness of the droplet properties occurs due to the crossing of particle paths. A set of model equations are studied but the technique is applicable to a more general and more physically correct set of equations. The effects of interesting numerical parameters such as mesh size, number of droplet characteristics, time step, and the injection pulse time are determined via a parameter study. In addition to confirming quadratic convergence, the results indicate slightly more sensitivity to grid spacing than to the number of characteristics.

INTRODUCTION

Theoretical modeling of the realistic spray combustion problems generally leads to a large system of partial differential equation. The gas phase properties such as the gas enthalpy, the gas species densities, and the turbulent scales are represented by a subsystem of parabolic equations. An Eulerian description of the liquid phase properties, i.e., droplet velocity, droplet radius, droplet surface temperature, and droplet number density leads to a set of hyperbolic equations with some tendency toward a parabolic character due to turbulent dispersion of droplets. A Lagrangian description of liquid phase properties will, however, lead to a subsystem of ordinary differential equations. These two subsystems of nonlinear coupled equations are generally so complex that a numerical solution with a high speed computer seems to be the only practical method. A realistic solution for a multidimensional unsteady turbulent spray combustion should include: a proper modeling of gas and particle turbulence, a complete chemical kinetics scheme, a proper accounting of gas dynamics–combustion interaction, a realistic description of the initial particle sizes and velocities (this will mainly be determined by the injector characteristics), effects of droplet secondary atomization, and a precise representation of the exchange laws

0021-9991/83 $3.00

between the phases, including the effects of transient droplet heating. A detailed comprehensive description of all the above phenomena may be an enormously expensive exercise. It may even be beyond the capabilities of present-day computers.

An alternative approach could be to start with an idealized situation, amenable to a practical treatment, and then incorporate more sophisticated models. However, every step towards a more comprehensive model will vastly increase the number of computations required. For example, a more complete description of chemical kinetics may require a large number of reactions involving a large number of species and thus making the equations highly stiff. Similarly, a proper description of the heat and mass exchange laws between the two phases can introduce enormous complexities. For example, in the study of Seth *et al.*, the conduction inside the droplet is the dominant mode of heat transfer. Unsteady transient heating of the droplets occurs with a prevaporization period preceding the period of significant vaporization for each droplet. During the prevaporization period the droplet is heated well above its initial temperature. Heating still continues after a significant vaporization rate begins. Even for this simple case, as many as fifteen additional differential equations were introduced for the case of monodispersed droplets. More comprehensive heat and mass exchange models, which may include the internal circulation, the polydisperse nature of droplets, and the multicomponent nature of fuel, can easily make the computation costs nonaffordable. Therefore, the need for improved numerical methods, through numerical experimentation, cannot be overemphasized.

In the present study, the numerical experimentation is performed by considering a system of model equations. In selecting a model problem, it is highly desirable to choose one which is as simple as possible, consistent with retaining the essential features which affect the computational efficiency. Thus the model equations used in the present study retain the mathematical character of the parent equations but are considerably simplified otherwise. It must be understood that the intent here is to develop a methodology for solving spray equations and not to develop an improved model of spray phenomena. For that purpose, the use of model equations is very convenient.

The nonlinearity of the parent equations is retained by considering nonlinear source terms in the equations: These source terms express the exchange rates between the phases. The gas phase properties are assumed to be represented by a parabolic heat-diffusion type equation. Three equations are considered to represent the liquid phase properties, i.e., the droplet size, the droplet velocity, and the droplet number density. The numerical experiments on these equations indicate that for the parabolic equation, an efficient finite difference approach is the one based on an ADI (alternating direction implicit) scheme involving the solution of a set of tridiagonal matrices. For droplet equations in Eulerian form, the existing finite difference techniques appear inadequate in certain situations which are important in spray combustion. For example, the droplet radius and liquid velocities often become multivalued functions, since droplet paths cross as the flow develops. This can be treated in a natural way be the method of characteristics, but it is very difficult to

handle by finite differences. Realize that the droplet or particle path and the characteristic lines for the hyperbolic equations are identical.

Note that multivaluedness of the solutions can also occur whenever the initial droplet size or droplet velocity distribution is polydisperse. This type of multivaluedness is usually treated by considering the polydisperse spray to be the sum of a finite number of superimposed monodisperse sprays. The type of multivaluedness that is emphasized herein, however, can occur with a monodisperse spray. In particular, it happens whenever particle paths cross. The first type of multivaluedness appears first in the inflow boundary condition and therefore is known a priori to occur allowing it to be treated readily in the above-mentioned manner. The second type of multivaluedness first appears in the interior of the calculation domain and cannot be predicted prior to calculation.

Covering Equations

The gas phase properties are governed by parabolic partial differential equations, whereas the droplet properties are governed by hyperbolic equations. We treat the latter by the method of characteristics and reduce it to ordinary differential equation. These two sets of equations are nonlinearly coupled because of the mass, momentum, and heat transfer between the phases. In the present study, the model system contains five equations: one parabolic equation for the gas phase scalar θ (temperature) and four ordinary differential equations for four unknowns (defined before Eq. (3)), n, $\underline{x}$, s, and $\underline{U}_l$. It may be noted that in a real system containing many gas species, the mass densities of various species will be given by the similar parabolic equations. The gas phase velocity as well as the droplet surface temperature are assumed to be known. Thus the momentum coupling is neglected for the gas phase; for the liquid phase it is properly taken into account. The set of model equations is nondimensionalized by using characteristic values of length, velocity, temperature, and droplet size. The characteristic values used are, respectively,

$$Z_c = 10 \text{ cm}, \qquad U_c = 100 \text{ cm/sec},$$
$$\theta_c = 500°\text{K}, \qquad R_c = 100\,\mu.$$

The nondimensional equation for θ in axisymmetric coordinates (r, z) can be written as

$$\frac{\partial \theta}{\partial t} = -\frac{\partial}{\partial z}(U\theta) + \frac{\alpha}{r}\frac{\partial \theta}{\partial r} + \alpha\left(\frac{\partial^2 \theta}{\partial r^2} + \frac{\partial^2 \theta}{\partial z^2}\right) - S_\theta, \tag{1}$$

where

$$S_\theta = \frac{K_1 n}{2\pi r\,\Delta r\,\Delta r}(1 + K_5(\theta - \theta_l))[1 + K_4[S(U - U_{l_z})^2 + U_{l_r}^2)]^{1/4}$$
$$\times S^{1/2} \ln(1 + K_5(\theta - \theta_l)), \tag{2}$$

the quantity $2\pi r\,\Delta r\,\Delta z$ represents the volume of a computational cell in an axisymmetric cylindrical geometry, and the subscript l represents a Lagrangian variable associated with any computational droplet. In the above equations, $U$and θ_l are assumed to be known constants. Thus the gas velocity is assumed to be uniform and in the axial direction. Consequently, the radial convection term does not appear in Eq. (1). Here S_θ stands for the nondimensional heat transfer rate between the phases. The variable K_1 represents the heat transfer time constant, and K_4 and K_5 are assumed to be constants. It should be noted that in physically realistic two phase situations, K_4 would represent the ratio of specific heat at constant pressure and the latent heat of vaporization, and K_5 would be the coefficient of the Reynolds number correction, where the Reynolds number is based on the droplet size and droplet velocity relative to the gas (see [1]). The equations for n, S, U_{l_z}, and U_{l_r} are described next.

Liquid Phase Equations

The liquid phase properties of interest are $\underline{U}_l$, the liquid velocity, $S = R^2$, where R is the droplet radius, and finally N, which is the number density of the droplets. The governing equations are of the hyperbolic type, and are usually written in the following form

$$\frac{\partial \underline{U}_l}{\partial t} + \underline{U}_l \cdot \nabla \underline{U}_l = \frac{K_3}{S^{1/2}} (\underline{U} - \underline{U}_l), \tag{3}$$

$$\frac{\partial S}{\partial t} + \underline{U}_l \cdot \nabla S = -K_2(1 + K_4[S((U - U_{l_z})^2 + U_{l_r}^2)]^{1/4}) \times \ln(1 + K_5(\theta - \theta_l)), \tag{4}$$

$$\frac{\partial N}{\partial t} + \nabla \cdot (\underline{U}_l N) = 0. \tag{5}$$

Observe that

$$n = Nv,$$

where n is the number of droplets associated with a given mass of liquid and v is total volume of gas and liquid per unit mass of liquid. A standard conservation argument show

$$\frac{\partial}{\partial t}\left(\frac{1}{v}\right) + \nabla \cdot \left(\frac{\underline{U}_l}{v}\right) = 0.$$

Hence (5) reduces to

$$\partial n/\partial t + (\underline{U}_l \cdot \nabla) n = 0. \tag{6}$$

These equations will be integrated using a Lagrangian formulation or equivalently, the method of characteristics. In particular, each Lagrangian variable at time t is given as $P = P(X_0, t_0; t)$, where X_0 and t_0 are the space and time coordinates at the point of injection. The position of a computational particle at time t is denoted by $\underline{X} = X(X_0, t_0; t)$. With this convention the above equations are formally equivalent to the following:

$$\frac{dn}{dt} = 0, \tag{7}$$

$$\frac{d\underline{X}}{dt} = \underline{U}_l, \tag{8}$$

$$\frac{dS}{dt} = -K_2(1 + K_4[S((U - U_{l_z})^2 + U_{l_r}^2)]^{1/4}) \times \ln(1 + K_5(\theta - \theta_l)), \tag{9}$$

$$\frac{d\underline{U}_l}{dt} = \frac{K_3}{S^{1/2}}(\underline{U} - \underline{U}_l). \tag{10}$$

Actually, Eqs. (3)–(5) are not the most general representation of the droplet behavior; Eqs. (7)–(10) are preferred in that multivalued solutions can be treated systematically. These multivalued solutions are common in two phase flows since droplet trajectories often intersect. Note therefore that Eqs. (7)–(10) are actually the primitive form and other restricted forms such as Eqs (3)–(5) are special cases.

Boundary and Initial Conditions

At the inflow ($z = 0$), the adiabatic boundary condition for θ is prescribed as

$$U_\infty \rho_\infty C_p \theta_\infty = U_0 \rho_0 C_p \theta_0 - \lambda(\partial\theta/\partial z)_{z=0},$$

which in the nondimensional form reduces to

$$\theta_\infty = \theta_0 - \alpha(\partial\theta/\partial z)_0; \qquad \alpha = \lambda/\rho C_p U_0 Z_0,$$

where θ_∞ is prescribed.

An outflow boundary condition is needed to make the computational domain finite. We use now the standard outflow conditions at these points [2]. Mathematically, it takes the form

$$\partial^2\theta/\theta z^2 = 0 \qquad \text{at} \quad z = 1$$

At the r boundary, the boundary conditions are

$$\partial\theta/\partial r = 0 \qquad \text{for} \quad r = 0 \quad \text{and} \quad r = 1.$$

Initially at time $= 0$, θ is assumed to be the same as θ_∞.

The droplet flow is assumed to be initially conical and flowing from a point source at a point on the axis of symmetry where $z < 0$. Initially, all the characteristics are positioned at $z = 0$. The initial values of S and n are assumed to be uniform, and U_l is obtained from the assumption of a conical flow.

Though the above initial conditions are highly idealized for the present study, the computer code has the flexibility to allow for more complicated initial conditions. The inflow boundary conditions in our example have been chosen to be single-valued (monodisperse spray) because we wish to study only multivaluedness due to the crossing of particle paths (or equivalently, characteristics). Such multivaluedness will occur in some of the cases studied.

Numerical Aspects and Solution Procedure

For the parabolic equation, an ADI (alternating direction implicit) scheme is used. Thus a full time advancement takes place in two steps. First, time is advanced by a half step in the z-orientation and then it is advanced by another half step in the r-orientation. The difference equations are

in the z-orientation

$$\frac{\theta^{n+1/2} - \theta^n}{\Delta t/2} = -\frac{\partial}{\partial z}(U_z \theta^{n+1/2}) + \frac{\alpha}{r}\frac{\partial}{\partial r}\theta^n + \alpha \frac{\partial^2}{\partial r^2}\theta^n + \alpha \frac{\partial^2}{\partial z^2}\theta^{n+1/2} - (S_\theta)^n,$$

and then the r-orientation

$$\frac{\theta^{n+1} - \theta^{n+1/2}}{\Delta t/2} = -\frac{\partial}{\partial z}(U_z \theta^{n+1/2}) + \frac{\alpha}{r}\frac{\partial}{\partial r}\theta^{n+1} + \alpha \frac{\partial^2}{\partial r^2}\theta^{n+1} + \alpha \frac{\partial^2}{\partial z^2}\theta^{n+1/2} - (S_\theta)^{n+1},$$

which is second-order accurate in Δr, Δz, and Δt. Because S_θ^{n+1} is nonlinear, it needs to be evaluated either by an iterative or quasilinearization procedure. One crude approximation is to take S_θ^{n+1} to be the same as S_θ^n. Then the results are less than second-order accurate in time. To obtain second-order accuracy in time, an iterative scheme is used, where S_θ^n is used as the initial approximation and is updated until the desired accuracy is obtained. In another method involving quasilinearized procedure, S_θ^{n+1} is written as

$$S_\theta^{n+1} = S_\theta^n + (\partial S/\partial \theta)^n(\theta^{n+1} - \theta^n).$$

In the first approximation θ^{n+1} is assumed to be the same as θ^n. Due to coupling from liquid phase equations, it is updated by iteration until desired accuracy is achieved.

The ordinary differential equations (7)–(10) are integrated over the same time step by a standard second-order predictor–corrector scheme [5]. The local values of temperature for Eq. (9) at each point on the trajectory are obtained from linear interpolation of the four surrounding values of the gas-phase solution in the computation cell through which the droplet is passing.

The energy interchanges occurring as the droplets traverse each grid cell are evaluated by superimposing to the four surrounding grid points as shown in Fig. 1. Therefore

$$S_\theta(I,J) = S_\theta(\text{Char.}) * \frac{\text{Volume I}}{\text{Total Cell Volume}},$$

ans $S_\theta(I+1,J)$, $S_\theta(I+1,J+1)$, and $S_\theta(I,J+1)$ are readily determined in analogous fashion.

Due to the linear interpolation, this maintains the second-order accuracy in our finite difference scheme, as opposed to the first-order accuracy that would result by assuming that the coefficients are constant in each cell [3, 4].

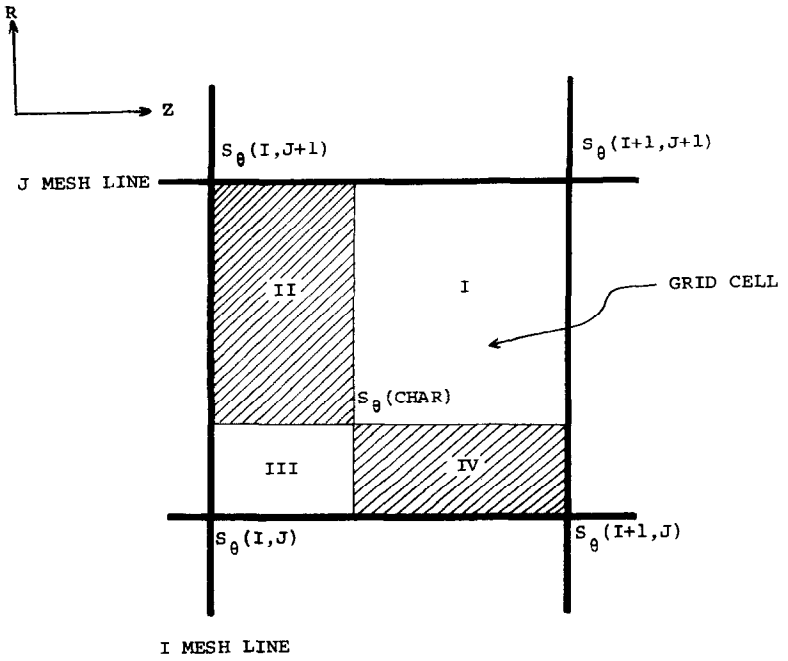

FIGURE 1

In the iteration cycle, the solutions for the liquid properties are first advanced one full time step via Lagrangian calculations and then the θ solution is advanced two half time steps in the ADI subcycle.

Numerical Results

In this section we discuss the results from selected numerical experiments, as well as the specific integration schemes used in these simulations. As noted above, two ways were considered for treating the nonlinearity S_θ in the θ equation, namely, iteration with respect to the source term S_θ and quasilinearization. The former has the advantage that the distribution scheme discussed above for the source term S_θ is physically clear. We found, however, that the number of iterations grew very rapidly with Δt, and the time step restrictions were far more severe than those required for reasonable engineering accuracy. The distribution scheme used in quasilinearization distributed S_θ and $\partial S_\theta/\partial\theta$ in exactly the same way S_θ was distributed in the iterative scheme. From a physical point of view this is somewhat ad hoc; however, in those cases where the iteration converged, the difference in the answers between the two approximations occurred in the fourth or fifts decimal place. Moreover, the CPU time required for the interative scheme was considerably higher than that required for the quasilinearization. *Thus all of the results presented below used the latter scheme.*

The computer code developed for these simulations can use a variety of schemes for integrating the ordinary differential equations (7)–(10) arising from the Lagrangian approach. To maintain a second-order approximation in our scheme, a preditor–corrector second order Runge–Kutta method was used to integrate (7)–(10).

Three grids were used in the calculations. The parameters varied were the number of characteristics N, the time step Δt, the grid spacings Δr and Δz, and finally the injection pulse time τ_p. (The physically continuous injection process is represented in discretized fashion by considering injection pulses with a period τ_p). Data for the individual grids is listed below:

coarse grid:	$N = 3$,	$\Delta t = 0.02$,	$\Delta r = \Delta z = 0.1$,	$\tau_p = 0.04$
base grid:	$N = 6$,	$\Delta t = 0.01$,	$\Delta r = \Delta z = 0.05$,	$\tau_p = 0.02$
finite grid:	$N = 24$,	$\Delta t = 0.005$,	$\Delta r = \Delta z = 0.025$,	$\tau_p = 0.01$

To get a rough idea of the order of accuracy of our approximations to the temperature field θ, we measured the discrete L_2 error at steady state, assuming that the fine grid approximation was exact. More precisely, letting θ_i denote the value of approximate temperature at the ith grid point (as computed on the coarse or based grid), and letting θ_i^E denote the analogous value for the fine grid, we then defined

$$E = \left(\sum_i |\theta_i - \theta_i^E|^2 \, \Delta z \, \Delta r \right)^{1/2}$$

as the measure of error, where the sum is over all grid points. On the coarse grid this error was 3.6×10^{-2} while on the base grid it was 4×10^{-3}. This demonstrates a quadratic convergence in our scheme in the sense that E is reduced by at least a factor of four (in this case it is nine) when the grid is cut in half.

We selected the results obtained from the base grid to illustrate various features of the flow. The results of that calculation are portrayed in Figs. 2–5 for gas temperature, droplet trajectories, and droplet size. The phenomenon modeled is unsteady but reaches a steady state after an initial transient period. At $t = 0.5$ (50 time steps), for example, the solution is in the midst of the transient while by $t = 3$ (300 time steps), a steady state has been well established. Figure 2 displays the gas temperature θ during the transient period ($t = 0.5$). Note that the gas temperature initially (at $t = 0$) was equal to 2.0; the effect of the vaporizing droplets is to cool the gas since energy is required for vaporization. The neighborhood of the origin is where injection occurs (see Figs. 4 and 5), droplet number is greatest, and the cooling effect is greatest. On account of large gradients in space and time in this neighborhood, sensitivity to mesh size and time step are most severe in this region. The gas temperature in this neighborhood decreases with time, so that the cooling effect becomes less severe as time proceeds. There seems to be potential for benefit from nonuniform grid and variable time step, but this possibility has not yet been explored.

Figure 3 demonstrates the steady-state ($t = 3$) gas temperature profile. The coldest region is along the axis of symmetry which is essentially the center of the spray cone. Again, even in the steady state, the largest gradients occur in the neighborhood of the origin.

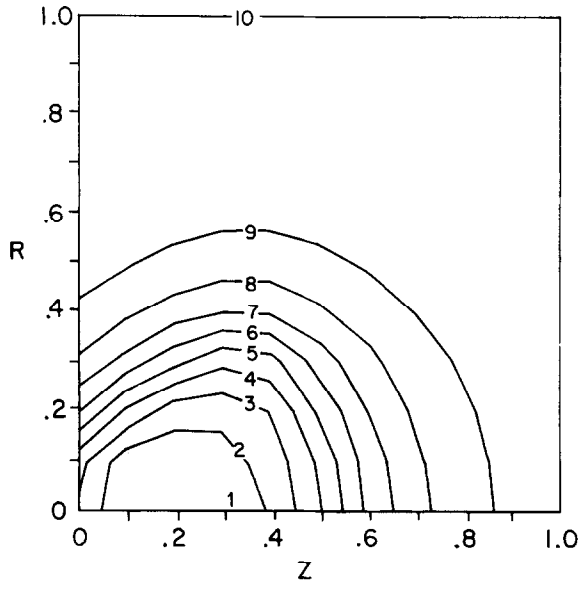

FIG. 2. Temperature contours (base case; time = 0.5).

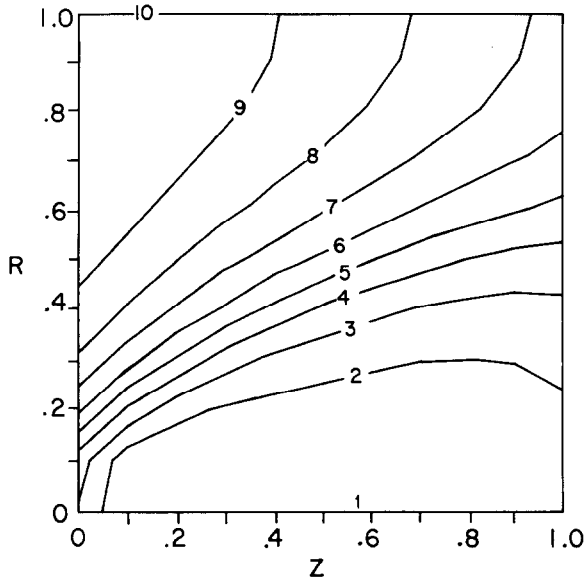

CONTOUR	VALUE
1	0.631742
2	0.778917
3	0.926092
4	1.073266
5	1.220441
6	1.367616
7	1.514791
8	1.661965
9	1.809140
10	1.956315

FIG. 3. Temperature contours (base case; time = 3.0, steady state).

Figures 4 and 5 show steady-state results for droplet size and droplet trajectories. Note that in Fig. 4, the circle radii represent droplet volume $S^{3/2}$ and not droplet radius $S^{1/2}$. Since a computer plots those circles with some degree of discretization of diameters, only the roughest inferences should be made from such graphs. The droplet size is definitely seen to decrease substantially as it moves through the hot gas. Of course, the droplets at the edge of the spray vaporize much more rapidly than the droplets in the spray center. The gas velocity is greater than the axial component of the initial droplet velocity so that drag causes the droplets to accelerate

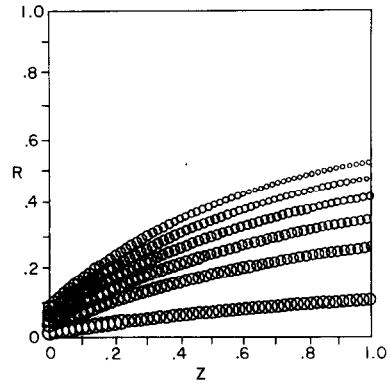

FIG. 4. Droplet volume (base case; time = 3.0).

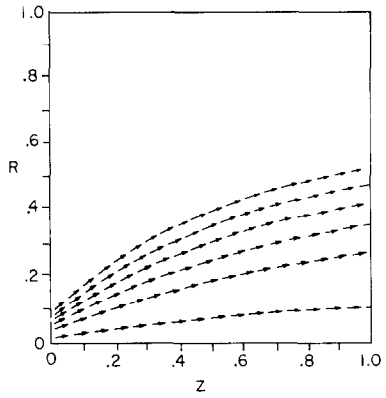

FIG. 5. Droplet velocity vector (base case; time = 3.0).

downstream. The trajectories are clearly seen to involve a turning of the droplets in that direction.

Note that the cell Reynolds number varied between 1.35 and 5.0 for all cases considered and, in particular, was 2.5 for the 20×20 mesh base case.

The next set of results is given in Figs. 6 and 7, and display the sensitivity of the approximation to changes in the number N of characteristics used and to the grid spacing Δz and Δr. In these figures comparisons are made with the results obtained from the base grid by varying one or more of these parameters. Figure 6 deals with

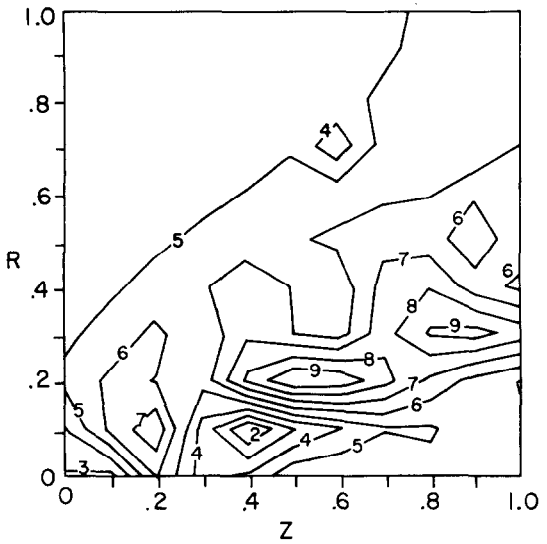

CONTOUR	VALUE
1	-0.022249
2	-0.015331
3	-0.008413
4	-0.001495
5	0.005423
6	0.012341
7	0.019259
8	0.026177
9	0.033095
10	0.040013

FIG. 6. Temperature difference contours (normalized change, three characteristics versus six characteristics; time = 3.0).

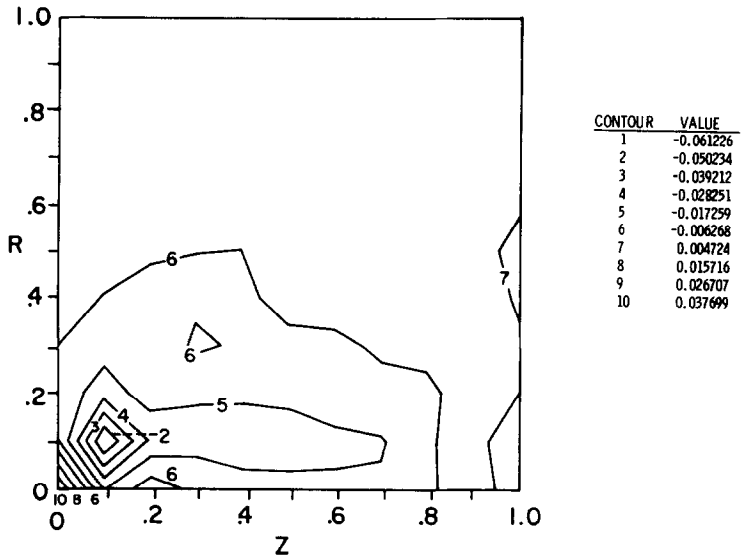

FIG. 7. Temperature difference contours (normalized change, 10×10 grid versus 20×20 grid; time = 3.0).

the case where the number of characteristics on the base grid has been changed from $N = 6$ to $N = 3$. Plotted are contours of constant values of

$$(\theta^{(6)} - \theta^{(3)})/\theta^{(6)},$$

where $\theta^{(6)}$ is the temperature field obtained from the base grid, and $\theta^{(3)}$ is the temperature field obtained from the base grid except where N has been reduced to 3.

Figure 7 has analogous contours except where the mesh spacing in the base grid has been changed from $\Delta r = \Delta z = 0.05$ to $\Delta r = \Delta z = 0.1$. These figures tend to indicate that the two-phase flow is satisfactorily resolved on the base grid, and in fact for most purposes, even the coarse grid may be satisfactory. They also show that the approximation is slightly more sensitive to the grid spacing than to the number of characteristics used.

Changes in the time step produce more delicate effects. First of all, the nature of the initial condition used places definite restrictions one the size of Δt, at least for small times t. The reason for this is that the sharp gradients produced near $t = 0$ may cause the calculated temperature to go negetive if Δt is too large. At this point, the calculations must be terminated due to the nature of the source terms. This, for example, was the case when Δt was increased in base grid from 0.02 to 0.05. It is to be emphasized that this restriction is far less severe than the restriction on Δt found in the iterative scheme.

Similar considerations show that the ratio $\tau_p/\Delta t$ must be sufficiently small. For example, if in the base grid (where $\Delta t = 0.01$, $\tau_p = 0.02$) the pulse time τ_p were increased to 0.05, then negative temperatures would occur.

Probably the most important feature of the Lagrangian formulation is demonstrated in Figs. 8 and 9. In this axisymmetric case, injection is considered to occur from a circular line source at $z = 0$. This may be viewed as the limit of a ring of injection orifices whereby both distances between orifices and orifices diameter go to zero. In this case, many intersections of droplet trajectories will occur (see Fig. 8) so that solutions for all droplet properties are multivalued. Note that the gas temperature, as shown in Fig. 9, is still single-valued. Any finite difference scheme based upon a continuum formulation employing Eqs. (3)–(5) could not represent this type of phenomenon. The crossing of the characteristic would not be allowed by a finite-difference scheme. Numerical diffusion would "merge" and "smear" the characteristics. In the case of a compressive wave in a gasdynamic field, such merging could give respectable global representation to shockwave formulation; however, in the present droplet study, such a result would be nonsensical. Again, with typical number densities, a negligibly small fraction of intersecting droplets will actually collide.

Finally, a comparison was made between the second-order distribution scheme discussed in this paper with the first-order scheme proposed by Gosman and Johns [3] and Dukowicz [4]. To do this, we retained all features of our discretization (ADI, method of characteristics, etc.) except for the replacement of the second-order distribution scheme with the first-order version. It is emphasized therefore that our comparison is with their proposed interpolation scheme to our model equations. It is not a comparison between their calculations and our calculations since different equations were employed. The latter had L_2 errors (using the fine grid as exact) 3.6×10^{-2} and 1×10^{-2} for coarse grid and base grid, respectively. This convergence is superlinear due to the fact that everything but the source term S_θ is treated with second-order accuracy, and that the coupling through S_θ is rather weak in this particular model. However, this convergence is definitely subquadratic, and theoretically should actually become linear as the grid spacings approach zero due to the first order treatment of S_θ. Further, it is worth mentioning that Crowe *et al.* [7]

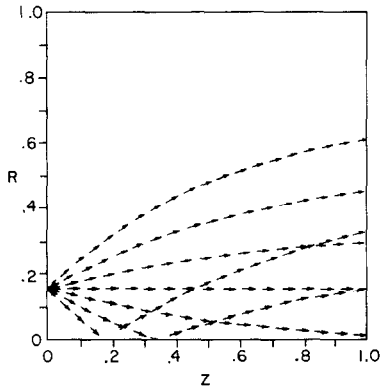

FIG. 8. Droplet velocity vector (circular line source case; time = 3.5, steady state).

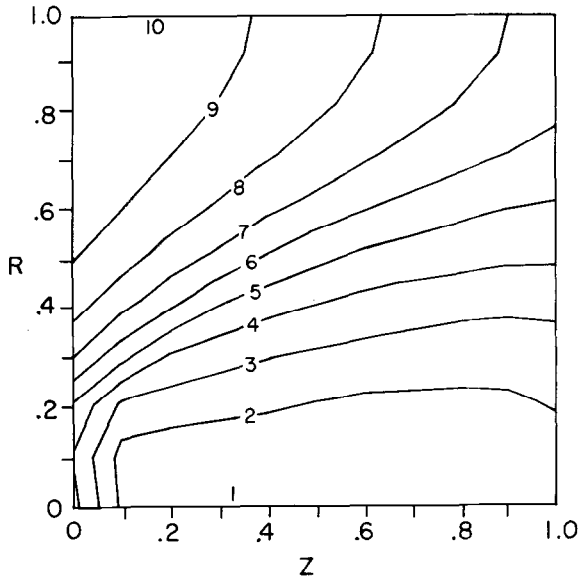

CONTOUR	VALUE
1	0.622950
2	0.770245
3	0.917540
4	1.064836
5	1.212131
6	1.359426
7	1.506721
8	1.654017
9	1.801312
10	1.948607

FIG. 9. Temperature contours (circular line source case; time = 3.5).

have used a source distribution scheme which is similar to that of Gosman and Johns [3] to solve steady-state spray equations. Since they are solving the steady-state two-dimensional planar equations as compared to the time-dependent axisymmetric equation used here, the present results cannot be compared with those of [7].

CONCLUSIONS

A system of model equations which retain the essential mathematical and numerical character of the parent equations for treating a typical two phase spray flow is employed. Through numerical experimentation on these equations, it is recommended that an Eulerian representation for the gas phase properties and a Lagrangian representation for the liquid phase properties be used with any spray model. See, for example, the model by Aggarwal *et al.* [6]. Indeed, for certain flow situations involving multivalued droplet properties, this seems to be the only appropriate approach. Following this approach, an efficient numerical algorithm is developed which is consistently second-order accurate. In this algorithm, the unsteady axisymmetric gas phase equations are solved by using a second-order accurate implicit ADI scheme, whereas the Lagrangian equations are solved by a second-order Runge–Kutta scheme. The treatment of exchange laws between the phases is also made second-order accurate by using two-dimensional linear interpolation and volume-weighted distribution. The results of two different numerical experiments are presented. In the first experiment, the sensitivity of those results to the changes in

time step, droplet pulse time, grid size, and number of groups of droplet characteristics used to describe the droplet injector is examined. All these results confirm a quadratic convergence as the grid size or the time step is varied. It may also be indicated that the results are slightly more sensitive with respect to the grid spacing than the number of characteristics.

The purpose of the second experiment was to demonstrate a physical situation which has multivalued droplet properties. For this case, a finite-difference solution of droplet equations based on an Eulerian description is inadequate. On the other hand, the Lagrangian description becomes a natural method for this type of flow. In addition, a comparison has been made between the interpolation scheme presented in this paper and the interpolation scheme proposed by Gosman and John [3] and Dukowicz [4]. With the latter scheme, which gives superlinear (but subquadratic) convergence, results are slightly inferior to those presented in this paper. Future computations of more realistic flows with relatively stronger two phase coupling might reveal more prominent differences between first- and second-order source function distribution.

ACKNOWLEDGMENTS

This research was supported by the Office of Basic Energy Sciences of the Department of Energy and by the Army Research Office.

REFERENCES

1. B. SETH, S. K. AGGARWAL, AND W. A. SIRIGNANO, *Combust. Flame* **39** (1980), 149.
2. G. FIX AND M. GUNZBURGER, *Comput. Math. Appl.* **3** (1977), 53.
3. A. D. GOSMAN AND R. J. R. JOHNS, "Computer Analysis of Fuel–Air Mixing in Direct–Injection Engines," SAE preprint 806091, 1980.
4. J. K. DUKOWICZ, *J. Comput. Phys.* **35** (1980), 229.
5. C. W. GEAR, "Numerical Initial Value Problems in Ordinary Differential Equations," Prentice–Hall, Englewood Cliffs, N. J., 1971.
6. S. K. AGGARWAL, G. J. FIX, D. N. LEE, AND W. A. SIRIGNANO, *in* "Proceedings of the Fourth IMACS Meeting on Advances in Computer Methods for Partial Differential Equations," IMACS, Brussels, 1981.
7. C. T. CROWE, M. P. SHARMA, AND D. E. STOCK, *Trans. ASME, J. Fluids Eng.* **99** (1977) (4), 325.